Atom probe study of phase transformations in a Ti-48 at.% Al alloy

Williams Lefebvre, Alain Menand, Annick Loiseau, Didier Blavette

Atom probe study of phase transformations in a Ti–48 at.% Al alloy

W. Lefebvre [a,*], A. Menand [a], A. Loiseau [b], D. Blavette [a]

[a] *Groupe de Physique des Materiaux, UMR CNRS 6634, Faculté des Sciences, Université de Rouen, Place Emile Blondel, 76821 Mont Saint Aignan, France*

[b] *Laboratoire d'Etude des Microstructures, UMR CNRS-ONERA, ONERA, BP 72, 29 av. de la Division Leclerc, 92322 Châtillon, France*

A Ti–48 at.% Al alloy has been investigated by means of atom probe field ion microscopy (APFIM) and transmission electron microscopy (TEM). Atom probe (AP) techniques have been used to determine the composition of the massive γ-phase (γ_m). The ultrafine lamellar structure, which consists of α_2- and γ-lamellae, has been also characterised. The α_2 plates in γ_m have been analysed with one-dimensional AP microscopy and observed in TEM. Their formation in γ_m seems to be induced by the presence of oxygen, which is rejected from the γ_m phase during the massive transformation. The influence of chemical order on the field evaporation process has also been studied for the $L1_0$-ordered structure of the γ_m phase.

Keywords: Atom probe; Ti–Al alloy; Two phase Ti–Al; Lamellar structures

1. Introduction

Because of their good high temperature properties, coupled with a low density, dual-phase ($\alpha_2 + \gamma$) titanium aluminides are one of the most promising materials for applications in the aerospace industry [1,2]. Since it is well known that macroscopic properties of a material are strongly related to its microstructure, many studies are aimed at controlling the microstructure by using additional elements associated with specific heat treatments [3,4]. However, the phase transformations involved in these alloys are still unclear. Moreover, the microstructure itself depends on the different possible transformation paths according to the thermal history of the alloy [5].

In this study, the results of some investigations performed on a binary $Ti_{52}Al_{48}$ model alloy are presented. One important feature of this alloy is that it well reproduces the behaviour of multicomponent alloys, such as GE type alloys [22], with respect to phase transformations. This alloy has been investigated by using two complementary techniques, atom probe field ion microscopy (APFIM) and transmission electron microscopy (TEM). The use of APFIM associated with TEM observations has made it possible to determine the phase composition as well as crystallographic structures at a near-atomic scale.

2. Experimental

The material studied is a Ti–48 at.% Al alloy (percentages are in at.% unless otherwise mentioned). The ingots were made by arc melting. Samples of these ingots were solution heat treated in a vertical furnace, under 1.2×10^5 Pa of argon, for 1, 16 or 48 h at 1683 K and then oil quenched. In order to perform APFIM analyses, heat treated samples were cut into $0.5 \times 0.5 \times 20$ mm^3 using electro-erosion. For tip preparation, as well as for TEM observations, each sample was electropolished in a 60% methanol, 34% butanol, 6% perchloric acid solution, at an average temperature of 233 K. The imaging gas for FIM observations was neon under a pressure of 3×10^{-3} Pa. Atom probe (AP) analyses were performed under a pressure of 10^{-8} Pa, with a tip temperature of 60 K, a pulse fraction of 19% and a

* Corresponding author. Tel.: +33-235-14-6653; fax: +33-235-14-6652.

E-mail address: williams.lefebvre@univ-rouen.fr (W. Lefebvre).

pulse repetition rate of 1.7 kHz. Three-dimensional AP microscopy analyses were performed with the tomographic AP developed at the University of Rouen [6]. TEM observations were performed in a Philips CM20.

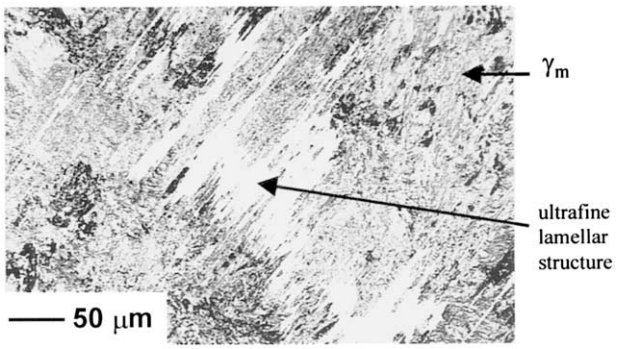

Fig. 1. Optical micrograph of a $Ti_{52}Al_{48}$ sample heat treated 16 h at 1410 °C and oil-quenched. The typical contrast of the γ_m-phase is clearly visible. The ultrafine lamellar structure is surrounded by the γ_m-phase.

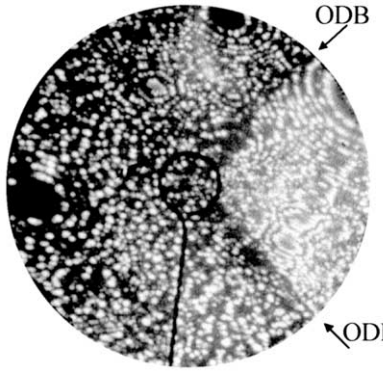

Fig. 2. FIM image of a sample heat treated 16 h at 1410 °C and oil-quenched. Two orientation domains of the γ_m-phase are evident.

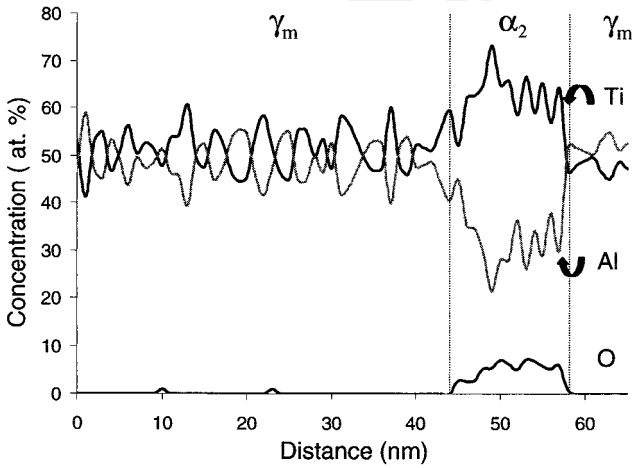

Fig. 3. Composition profiles in a $Ti_{52}Al_{48}$ alloy heat treated 1 h at 1410 °C and oil-quenched. The first part of the composition profiles corresponds to the γ_m-phase. The oxygen-rich region may be an α_2 plate.

3. $\alpha \rightarrow \gamma$ Massive transformation

The central part of the binary phase diagram of the Ti–Al system used for this study is the one given by McCullough et al. [7]. For a slow cooling rate from the α single-phase field (α is a hexagonal compact disordered phase) the first phase transformation that occurs is $\alpha \rightarrow \alpha + \gamma$. The γ-phase is a $L1_0$-ordered structure. This last transformation produces a lamellar structure in the former α-grains. At lower temperature, ordering takes place within α which transforms into α_2 (DO_{19}). Thus, the near-equilibrium state of the $Ti_{52}Al_{48}$ alloy at a low temperature consists in a dual-phase ($\alpha_2 + \gamma$) lamellar structure, with a small volume fraction of α_2 (less than 10%).

If the cooling rate from the α-phase field is sufficiently high (e.g. an oil-quench), the $\alpha \rightarrow \gamma$ massive transformation occurs [5,9]. During this transformation, the primary α-phase rapidly transforms into a massive γ-structure, containing a large amount of linear and planar defects. This transformation is assumed to occur at the average temperature of 1270–1370 K, depending on the cooling rate and on the composition [5,9,10]. Nevertheless, this transformation is usually not complete and the untransformed α regions later transform into an ultrafine lamellar structure [12,13,15], consisting of α_2 and γ-lamellae. The optical micrograph obtained after the $\alpha \rightarrow \gamma$ massive transformation of the material (Fig. 1) reveals the presence of an ultrafine lamellar structure surrounded by the massive γ_m-phase.

3.1. Massive γ-structure

The FIM image shown in Fig. 2 is related to the γ_m-phase. Two regions with different contrasts are separated by an orientation domain boundary (ODB). From one region to the other, there is only a change in the orientation of the [001] axis of the $L1_0$-ordered structure. This contrast is a consequence of the anisotropy of the $L1_0$-ordered structure, which can be described as a stacking of pure alternating planes along the [001] direction. As a result, the [001] substructure direction of the γ-phase appears in bright contrast, because of the difference of evaporation field that exists between Ti and Al layers along the [001] direction. Moreover, the alternating of bright and dim rings of the [001] pole is clearly visible.

A γ_m region was analysed using one-dimensional AP microscopy. The composition profiles shown in Fig. 3 reveals an oxygen-rich region, corresponding to a local enrichment in Ti. The composition of γ_m was found in a good agreement with previous AP analyses [11], i.e. a near equiatomic composition with a small amount of oxygen (Table 1). The oxygen-rich region is thought to be an α_2 plate [11]. In order to corroborate this result, a TEM observation was performed. The bright field

Table 1
Compositions of the γ_m- and α_2-phases analysed by 1DAP

	Ti (at.%)	Al (at.%)	O (at.)
γ_m	51.3 ± 1.7	48.7 ± 1.7	450 ± 400 ppm
α_2	63.9 ± 3.4	30.1 ± 3.2	6.0 ± 1.7%

image of a γ_m region shown in Fig. 4a reveals several plates appearing in dark contrast along two distinct directions. The identification of these plates as the α_2-phase was performed with use of dark field images (Fig. 4b and c). The vectors of the reciprocal lattice of the γ_m structure indicate that the α_2 plates have precipitated along two {111} closed-packed planes of the γ_m-phase. The crystallographic relationships between the α_2 plates and the γ_m-phase are the same as that in the lamellar structure [8]. As a result, these α_2 plates cannot be the product of the former α-phase. It has been proved that no simple orientation relationship exists between γ_m-phase and the former α grain where the massive transformation occurred [9,16]. The α_2 plates observed by 1DAP and TEM are thought to appear during or just after the massive transformation, but not before.

3.2. Ultrafine lamellar structure

As shown in Fig. 1, the massive transformation is not complete. Some regions of the former α-phase transform into an ultrafine lamellar structure consisting of α_2 and γ-lamellae [12,13,15]. A FIM image of the ultrafine lamellar structure shown in Fig. 5 exhibits the presence of two γ-lamellae with the same orientation. Two thin lamellae appearing in bright contrast are evident and are thought to be α_2 lamellae. A 3DAP analysis of the ultrafine lamellar structure has been performed (Fig. 6). Oxygen enrichment is related to the presence of a 5-nm-thick α_2 lamellae. Composition profiles across the lamellae (Fig. 7) indicate that the oxygen concentration in the α_2 lamellae reaches 4.1 at.%.

3.3. Saturation values of oxygen concentration in α, α_2 and γ

The main assumption for the estimation of the maximum oxygen concentration in each phase is that only Ti_6 octahedral cavities can be occupied by oxygen [11]. As a result, the maximum concentration of oxygen in each phase can be deduced from the amount of Ti_6 octahedral cavities.

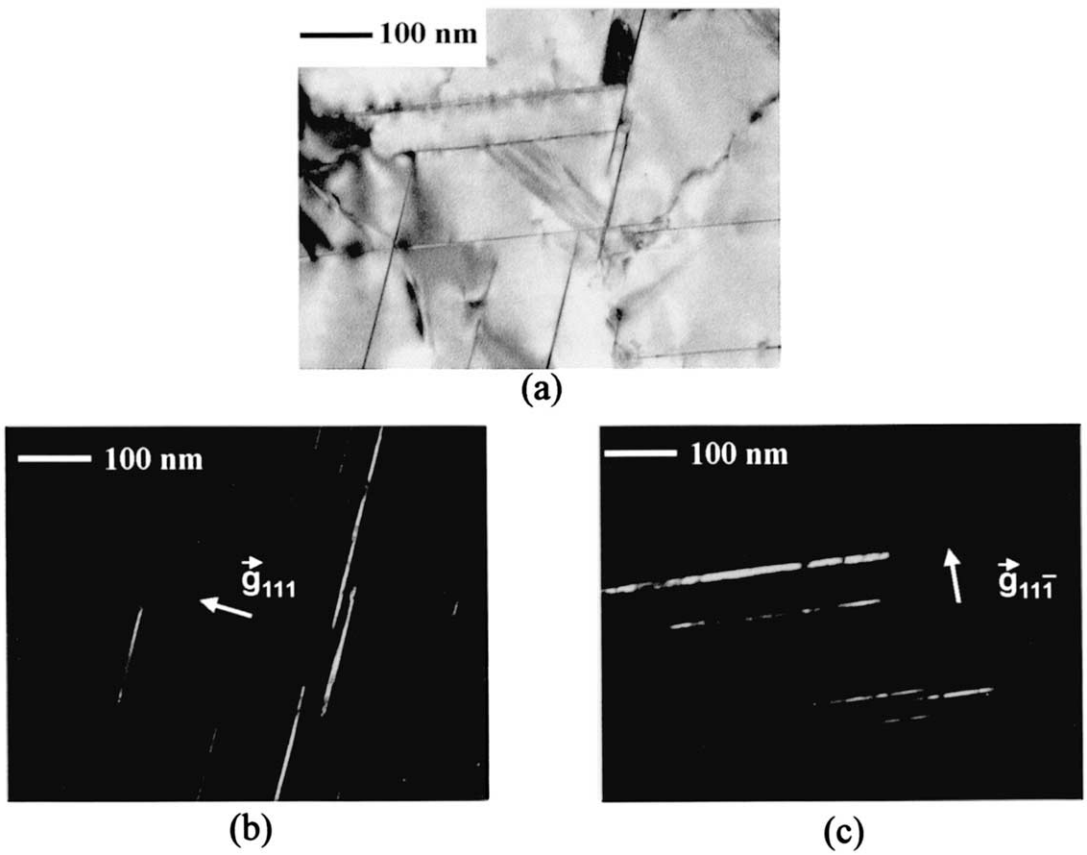

Fig. 4. TEM images of a $Ti_{52}Al_{48}$ sample heat treated 16 h at 1410 °C and oil-quenched. (a) Bright field image of a γ_m region performed with $\vec{z} = \langle 202 \rangle$. (b) $[\bar{2}201]$ Dark field of α_2 plates in the same region, performed with $\vec{z} = \langle 1120 \rangle_{\alpha 2} // \langle 202 \rangle_\gamma$ and $(0001)_{\alpha 2} // (111)_\gamma$. (c) $[\bar{2}201]$ Dark field of α_2 plates in the same region, performed with $\vec{z} = \langle 1120 \rangle_{\alpha 2} // \langle 202 \rangle_\gamma$ and $(0001)_{\alpha 2} // (11\bar{1})_\gamma$.

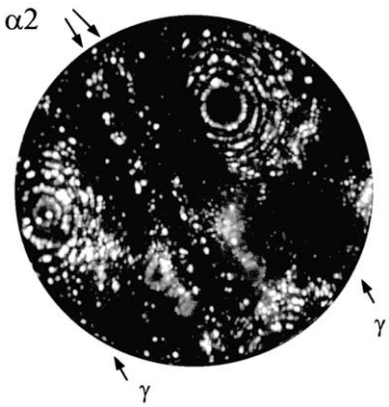

Fig. 5. FIM image of the ultrafine lamellar structure realised in a $Ti_{52}Al_{48}$ sample heat treated 48 h at 1410 °C and oil-quenched. γ-Lamellae are visible on both sides of the image. Thin α_2 lamellae are visible in the centre of the image.

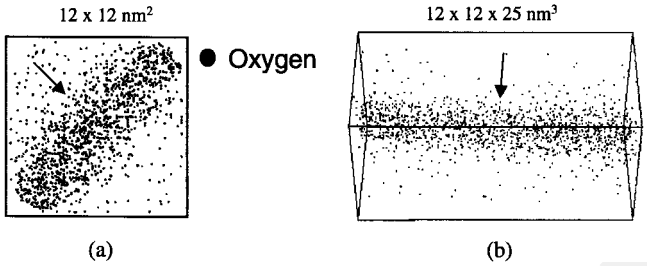

Fig. 6. 3DAP reconstruction of the ultrafine lamellar structure of a $Ti_{52}Al_{48}$ sample heat treated 16 h at 1410 °C and oil-quenched. Only oxygen atoms are drawn. (a) Front view. (b) Side view.

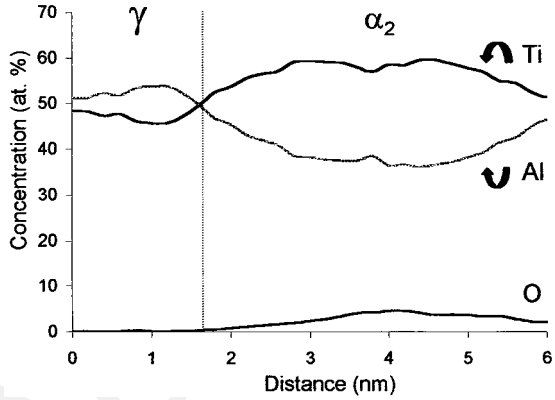

Fig. 7. Composition profiles drawn perpendicularly to the lamellar interface of the lamellae visible on Fig. 6.

Table 2
Estimated values of the maximum oxygen concentration in α and α_2, as a function of the concentration in Ti on substitutional sites

Ti (at.%)	52	55	60	65	70	75
$X(\alpha)$ (at.%)	2.0	2.7	4.5	7.0	10.5	15.1
$X(\alpha_2)$ (at.%)	2.8	3.8	6.2	9.6	14.2	20.0

3.3.1. Oxygen in the α-phase

One octahedral cavity exists per atom in the α-phase. Since this phase is disordered, substitutional sites are equivalent. Thus, the probability for an atom to occupy a substitutional site is equal to its concentration. The probability for an octahedral cavity to be a Ti_6 cavity is equal to the Ti concentration (C(Ti)) on substitutional sites to the power six. Therefore, the saturation value $X(\alpha)$ for the oxygen concentration in α is:

$$X(\alpha) = \frac{C(\mathrm{Ti})^6}{1 + C(\mathrm{Ti})^6}$$

3.3.2. Oxygen in the α_2-phase

Because of the chemical order of the α_2-phase, all substitutional sites are not equivalent but can be separated into Ti sites and Al sites. As a result, there exists one possible Ti_6 cavity for four atoms in this phase. The probability $P(\alpha_2)$ for one of these cavities to be surrounded by six Ti atoms is:

$$P(\alpha_2) = \left[\frac{4}{3} C(\mathrm{Ti})\right]^6$$

As a result, the number of Ti_6 octahedral cavities for one atom on substitutional site is:

$$N = 0.25 \times P(\alpha_2)$$

N only depends on the concentration of Ti on substitutional sites (C(Ti)), which is not exactly the same value than the concentration measured after an AP analysis.

The saturation value $X(\alpha_2)$ for the oxygen concentration in α_2 is given by:

$$X(\alpha_2) = \frac{0.25 \times P(\alpha_2)}{1 + 0.25 \times P(\alpha_2)}$$

3.3.3. Oxygen in the γ-phase

For an equiatomic composition, no Ti_6 octahedral cavity exists in the γ-phase. But for a $Ti_{50+\delta}Al_{50-\delta}$ composition in the γ-phase (if only substitutional sites are considered), i.e. a weak excess in Ti, a few Ti_6 cavities should exist. Assuming that excess Ti atoms are randomly distributed within the aluminium sublattice, octahedral Ti_6 therefore form in the (002) Ti pure planes of the $L1_0$-ordered structure. In such a case, the Ti concentration in the aluminium sublattice should be equal to 2δ. Since one possible Ti_6 cavity exists for two atoms in γ, the saturation value $X(\gamma)$ for the oxygen concentration in γ is given by:

$$X(\gamma) = \frac{0.25(2\delta)^2}{1 + 0.25(2\delta)^2}$$

Estimated saturation values for the oxygen concentration in α, α_2 and γ are summarised in Tables 2 and 3.

Table 3
Estimated values of the maximum oxygen concentration in γ, with a $Ti_{50+\delta}Al_{50-\delta}$ composition on substitutional sites

Ti (at.%)	50	51	52
$X(\gamma)$ (at.)	0	200 ppm	800 ppm

3.4. Oxygen's behaviour during the massive transformation

Oxygen is an interstitial impurity present in the α-phase before the massive transformation, with an average concentration of about 2000 at. ppm in industrial alloys [11]. It is now well known that the γ-phase cannot contain more than a few hundred at. ppm of oxygen [11]. This value is in good agreement with the estimations shown in Table 3. Oxygen will therefore be rejected from the γ_m-phase, during the massive transformation. The oxygen behaviour during the massive transformation remains unclear. This interstitial element was assumed to segregate on some defects of the γ-phase [19]. As oxygen of the former α-phase is rejected from the γ_m-phase during the massive transformation, this is likely to induce the precipitation of α_2 plates inside the γ_m-phase.

The number N of Ti_6 octahedral cavities per atom on substitutional site have been compared with the number N' of oxygen atoms per atom on substitutional sites. According to the results shown in Table 1, the concentrations on substitutional sites are 68 at.% Ti and 32 at.% Al. For such concentrations, the value of N is 13.9%, that means 13.9% of Ti_6 octahedral cavities for one atom on substitutional site. According to the 1DAP analysis (Fig. 3 and Table 1), N' is equal to 6.3%. Therefore, Ti_6 cavities are thought to be half-occupied by oxygen atoms inside the α_2 plate observed in γ_m. This may influence the volume fraction of α_2 in γ_m.

From the composition profiles drawn across the α_2 lamellae analysed using 3DAP, we find an average concentration of 59 at.% Ti and 4.1 at.% O inside α_2. From these values, one can deduce $N = 7.6\%$ and $N' = 4.3\%$. Accounting for statistical errors, these values can also correspond to an occupation of one Ti_6 octahedral cavity in two.

4. Influence of the chemical order of the γ-phase on the field evaporation

As shown in Section 1.1, the chemical order in the γ-phase gives rise to a contrast in FIM images. This is a consequence of two effects. One is the anisotropy of the $L1_0$-ordered structure. The other is the difference between the evaporation fields of Ti and Al atoms. The {100) planes of the γ-structure have an equiatomic composition contrary to the (002) planes which are pure planes of either Ti or Al. Thus, the two ⟨100] directions are not equivalent to the [001] direction with respect to the evaporation process.

A FIM image taken along the [001] direction of the γ_m structure (Fig. 8a) reveals bright rings, assumed to be Ti pure planes, which are cut by a dark plate. The 3DAP analysis performed at the centre of this region is shown in Fig. 8b. This analysis clearly shows a small region, which has a higher density. This observation is in good agreement with the contrast observed in Fig. 8a. The dark contrast in FIM is related to a lower evaporation field compared with the bright planes of the γ-structure. This local difference in the evaporation field induces local magnification [17,18].

The curves of Fig. 9 have been drawn across the interface between the two regions, as shown by the arrow of Fig. 8b. The composition profile of Fig. 9 can be separated into three regions. The first one, because

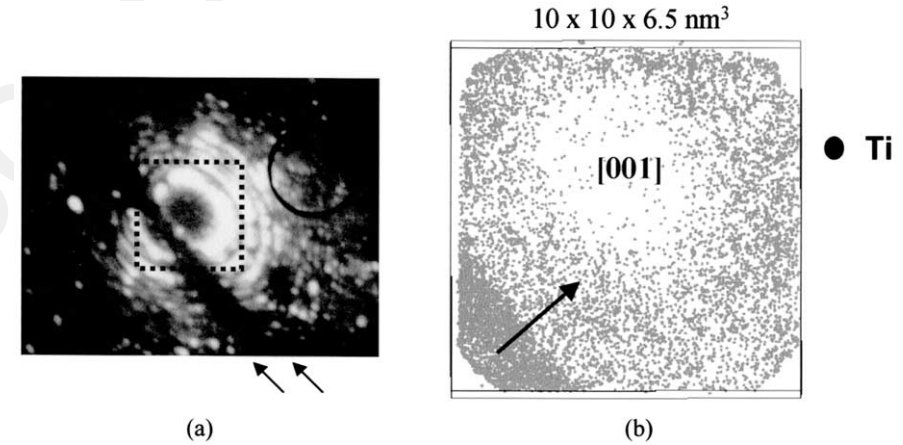

Fig. 8. (a) FIM image realised in a $Ti_{52}Al_{48}$ sample heat treated 16 h at 1410 °C and oil-quenched. Bright rings corresponding to the [001] axis of the γ-phase are clearly visible. Those rings are cut by a dark plate shown by arrows. (b) 3DAP reconstruction of the same sample performed along the [001] axis within the dotted square drawn in (a).

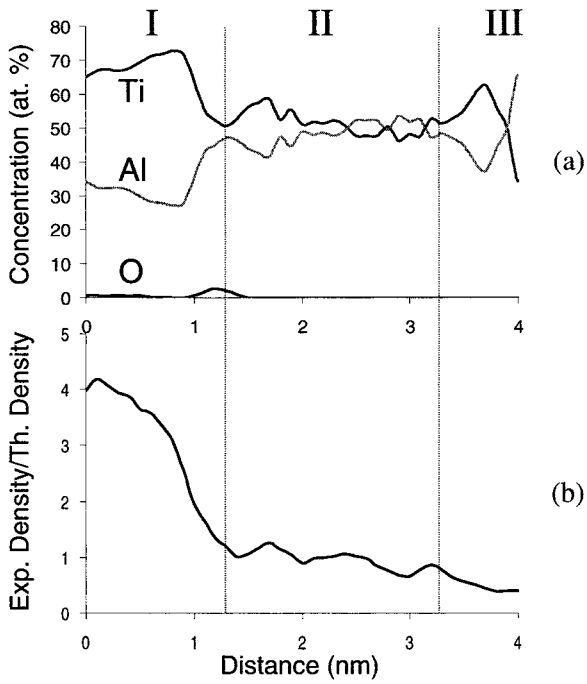

Fig. 9. (a) Composition profiles across the interface between the low and high evaporation field region as shown by the arrow of Figure 10b. (b) Corresponding fluctuations in the local density of atoms in the same region. The ratio between the experimental density of atoms and the theoretical density is plotted upon the distance.

of its high density (Fig. 9b), is a low evaporation field region. In region II, the density of atoms is in good agreement with the density expected for this material. In addition, the near equiatomic composition of γ_m is obtained. The density in region III is lower. This is due to a local depletion close to the [001] pole. Because of this depletion, significant fluctuations in the concentrations are observed.

Region I has a significantly higher concentration in Ti, associated with a small amount of oxygen, which is detected as TiO^{2+} ions. Therefore, it might be tempted to conclude that this region is the α_2-phase. However, the oxygen detected in this region (8600 at. ppm) may also be a consequence of the low evaporation field. Indeed, a few TiO^{2+} ions are detected for such analyses conditions in the γ-phase. That is not the case when the optimal evaporation field is reached. Moreover, the α_2-phase is known to have a higher evaporation field than the γ-phase. As a consequence, the dark region cannot correspond to the α_2-phase, otherwise the contrast of the FIM image, as well as the density of atoms in the 3DAP volume (Fig. 9b), would have been opposite to those observed.

According to Larson et al. [14] and Abe et al. [20], this darkly imaged region could also be the γ-phase with another orientation. FIM images of the γ-phase, with a similar contrast, have been obtained by Larson and Miller [14] in a TiAl-based alloy with a near-lamellar microstructure. This contrast was found to be due to in situ micro-twinning of γ, inside the field ion microscope. However, the γ_m-phase contains much more defects than the γ-phase of the near-lamellar microstructure [9,16]. As a consequence, the dark contrast of Fig. 8a could correspond to another kind of defects. Using HRTEM, Abe et al. have shown that, between two antiphase domains of γ_m, there can exist a thin region (a few nanometer thick) where the [001] axis is perpendicular to the [001] axis of the two adjacent antiphase domains. The FIM image (Fig. 8a) could not be used to determine whether the two bright regions have an antiphase domain relationship. Nevertheless, the assumption suggested by Abe et al. seems to better correspond to our observation.

Thus, the difference in the evaporation field at the surface of the analysed sample can be attributed to a difference in the orientation of the [001] axis of the γ-structure, which induces a change in the composition measured after the evaporation of the surface of the tip. As a result, the high concentration of Ti in the low evaporation field region could be due to a selective loss of Al. Indeed a significant amount of Al^+ and AlH^+ ions were detected in this region. That means that the evaporation field in this region was low enough to prevent a significant number of Al^+ ions to be post-ionised [21]. That also means that the evaporation field was low enough to allow hydrogen to associate with Al atoms before their evaporation. This association between Al and H atoms is assumed to be the main reason for the selective loss of Al, since it permits preferential evaporation of Al atoms.

5. Conclusion

APFIM analyses, as well as TEM observations, of a massively transformed Ti–48 at.% Al alloy have been successfully performed. The results presented in this study have provided a better understanding of the oxygen behaviour during the $\alpha \rightarrow \gamma$ massive transformation. It has indeed been shown that α_2 plates can precipitate during or just after the massive transformation, within the γ_m-phase. This precipitation is thought to be induced by the presence of oxygen, which is rejected from the γ_m-phase during massive transformation. The effect of chemical order on the field evaporation in 3DAP has been also shown. Chemical order induces fluctuations in the evaporation field and may lead to biased compositions.

Acknowledgements

We gratefully acknowledge Dr S. Naka and Dr M. Thomas for providing samples and for helpful discussions and comments.

References

[1] Y.W. Kim, Intermetallics 6 (1998) 623.
[2] Y.W. Kim, Acta Mater. 40 (1992) 1121.
[3] S.C. Huang, E.L. Hall, Metall. Trans. 22A (1991) 427.
[4] S.C. Huang, D.S. Et Shih, in: Y.W. Kim, R.R. Boyer (Eds.), Microstructure/Property Relationships in Titanium Aluminides and Alloys, TMS, Warrendale, PA, 1993, p. 299.
[5] S.A. Jones, M.J. Kaufman, Acta Met. 41 (1993) 387.
[6] D. Blavette, J.-M. Sarrau, B. Deconihout, A. Menand, Nature 363 (1993) 432.
[7] C. McCullough, J.J. Valencia, C.G. Levi, R. Mehrabian, Acta Met. 37 (1989) 1321.
[8] M.J. Blackburn, The Science, Technology and Applications of Titanium, Pergamon Press, Oxford, 1970, p. 633.
[9] P. Wang, G.B. Viswanathan, V.K. Vasudevan, Met. Trans. A 23A (1992) 690.
[10] D. Veeraraghavan, P. Wang, V.K. Vasudevan, Acta Mater. 47 (1999) 3313.
[11] A. Menand, A. Huguet, A. Nérac-Partaic, Acta Mater. 44 (1996) 4729.
[12] K. Hono, E. Abe, T. Kumagai, H. Harada, Scr. Met. 35 (1996) 495.
[13] E. Abe, T. Kumagai, M. Nakamura, Phil. Mag. Lett. 72 (1995) 291.
[14] D.J. Larson, M.K. Miller, Mater. Sci. Eng. A250 (1998) 72.
[15] T. Kumagai, E. Abe, M. Takeyama, M. Nakamura, MRS Symp. Proc. 364 (1995) 181.
[16] A. Denquin, Ph.D. thesis, University of Lille, 1994.
[17] M.K. Miller, M.G. Hetherington, Surf. Sci. 246 (1991) 442.
[18] F. Vurpillot, A. Bostel, D. Blavette, Appl. Phys. Lett. 76 (21) (2000) 3127.
[19] B.K. Kad, H.L. Fraser, Phil. Mag. Lett. 70 (1994) 211.
[20] E. Abe, N. Nakamura, Phil. Mag. Lett. 75 (1997) 65.
[21] R. Haydock, D.R. Kingham, Phys. Rev. Lett. 44 (23) (1980) 1520.
[22] US Patent no. 4879092 (1989).